The evolution of the fraction of Er ions sensitized by Si nanostructures in silicon-rich silicon oxide thin films

2009 Nanotechnology 20 355704

(http://iopscience.iop.org/0957-4484/20/35/355704)

Nanotechnology **20** (2009) 355704 (8pp) doi:10.1088/0957-4484/20/35/355704

The evolution of the fraction of Er ions sensitized by Si nanostructures in silicon-rich silicon oxide thin films

P Noé[1], H Okuno[1], J-B Jager[1], E Delamadeleine[1], O Demichel[1], J-L Rouvière[1], V Calvo[1], C Maurizio[2] and F D'Acapito[2]

[1] INAC/SP2M, Commissariat à l'Energie Atomique-MINATEC, 17 rue des Martyrs, F-38054 Grenoble Cedex, France
[2] CNR-INFM-OGG c/o ESRF, GILDA-CRG, BP 220, F-38043 Grenoble, France

Received 16 March 2009
Published 12 August 2009
Online at stacks.iop.org/Nano/20/355704

Abstract

Photoluminescence (PL) and time-resolved PL experiments as a function of the elaboration process are performed on Er-doped silicon-rich silicon oxide (SRO:Er) thin films grown under NH_3 atmosphere. These PL measurements of the Er^{3+} emission at 1.54 μm under non-resonant pumping with the Er f–f transitions are obtained for different Er^{3+} concentrations, ranging from 0.05 to 1.4 at.%, and various post-growth annealing temperatures of the layers. High resolution transmission electron microscopy (HRTEM) and energy-filtered TEM (EFTEM) analysis show a high density of Si nanostructures composed of amorphous and crystalline nanoclusters varying from 2.7×10^{18} to 10^{18} cm^{-3} as a function of the post-growth annealing temperature. Measurements of PL lifetime and effective Er excitation cross section for all the samples under non-resonant optical excitation with the Er^{3+} atomic energy levels show that the number of Er^{3+} ions sensitized by the silicon-rich matrix decreases as the annealing temperature is increased from 500 to 1050 °C. The origin of this effect is attributed to the reduction of the density of sensitizers for Er ions in the SRO matrix when the annealing temperature increases. Finally, extended x-ray absorption fine-structure spectroscopy (EXAFS) shows a strong correlation between the number of emitters and the mean local order around the erbium ions.

(Some figures in this article are in colour only in the electronic version)

1. Introduction

Ionized rare earth (RE) incorporation in semiconductors and glasses has received increasing attention over the last 20 years because of their potential applications in optoelectronics [1]. In particular, Er^{3+}-doped materials are of particular interest due to the $^4I_{13/2} \rightarrow {}^4I_{15/2}$ transition at 1.54 μm within the Er^{3+} 4f shell, corresponding to the minimum absorption loss in optical fibres and the possibility of optical gain when incorporated into glass hosts. Silicon has been one of the most studied hosts [2] for Er because of the possibility of photonic–electronic integration. Various silicon-based hosts for Er^{3+} ions have been studied and Si nanoclusters and luminescence centres (Si-ncs and LCs) incorporated with erbium in a silicon oxide matrix (silicon-rich silicon oxide) have recently attracted much attention from the scientific community due to their larger photoluminescence (PL) yield for Er than that of SiO_2 or monocrystalline silicon [3, 4]. Indeed several groups reported PL intensities two orders of magnitude higher in Er-doped silicon-rich oxide (SRO:Er) than in an SiO_2 matrix [5] as a result of an increased effective Er excitation cross section via the SRO matrix in comparison with direct photon absorption by the Er^{3+} 4f transitions [6]. Moreover the interaction between Si-ncs/LCs and Er^{3+} is strongly influenced by the distance between them [7]. Thus it has been demonstrated [8] that Er^{3+} can be more efficiently excited by a network of amorphous and interconnected Si-ncs in the oxide matrix instead of well-separated ones. But the Si-ncs, which act as sensitizers for Er ions, and introduced by the Si excess, have two opposite effects on the Er^{3+} optical properties: it enhances the Er excitation but, on the other hand, it creates non-radiative pathways which are detrimental to the Er^{3+} radiative relaxation [9]. But, in spite of the large sensitizing effect of Si-ncs for Er^{3+}, several reports showed that only a small fraction (less than 1/10) of the Er ions in SiO_x layers can be excited due to the small interaction volume around Si-ncs [10] or to the excited state

absorption [11]. Therefore a compromise has to be found between the fraction of Er ions which can be sensitized by the Si-ncs, which depends, amongst other parameters, on the Si excess in the oxide, and the Er luminescence lifetime which is decreased by the introduction of detrimental defects when the Si excess increases. However, first reports of optical gain from SRO:Er waveguides have been reported and demonstrate the great potentiality of such materials [12, 13]. But net optical gain has not been achieved yet, due to the limited fraction of the population of Er^{3+} ions which can be sensitized in the SRO matrix.

In this work, the PL properties of original SRO:Er layers grown under NH_3 atmosphere with high Si contents (43–44 at.%) are investigated as a function of the Er concentration C_{Er} and the post-deposition annealing temperature T_a. TEM and EFTEM analyses show a high density of silicon nanostructures varying as a function of the annealing temperature of the layers. Time decay and effective excitation cross sections of Er^{3+} ions in these SRO:Er thin films, obtained under non-resonant pumping excitation, are shown to be dependent on the elaboration parameters of the layers. In particular, the number of Er^{3+} emitters is highly influenced by the C_{Er} and the T_a of the SRO:Er layers. Extended x-ray absorption fine-structure spectroscopy (EXAFS) has been revealed to be a powerful tool in the study of the Er environment in glasses and semiconductors. In this study, EXAFS investigations are showing a strong correlation between the local structure around Er atoms and the evolution of the number of excited erbium ions as a function of the annealing temperature, giving an alternative explanation as to what has already been reported in the literature concerning the limited fraction of Er^{3+} ions sensitized by SRO matrices.

2. Experimental details

The SRO:Er layers were obtained by co-evaporation of an SiO load and metallic Er pellets under NH_3 atmosphere in a high vacuum vessel [14]. In previous studies [7], we have shown by extended x-ray absorption fine structure that the use of NH_3 reduces noticeably the Si–Er interatomic distances, which results in a strong enhancement of the PL properties under non-resonant pumping. This result is due to the high density of sensitizers in such an SiO matrix and the improved sensitization efficiency of Si-ncs/LCs for Er^{3+} ions when the deposition is made under NH_3. This improved sensitization efficiency is characterized by a higher PL efficiency of these recombination centres in the visible and near-IR range. The Si-ncs and LCs are obtained by annealing the SRO matrix after thin film deposition. Thermal annealing enhances the luminescence efficiency of the SiO matrix due to the phase separation of SiO into Si aggregates in pure SiO_2. The LCs are light-emitting defects due to highly localized defect states in silica induced by the excess-silicon-related electronic defects. For example, they are generally attributed to O deficiencies as a result of the nonstoichiometric composition of SRO.

In order to investigate the optical properties of these Er-doped SRO layers, 400 nm thick SiO:Er thin films with different Er concentrations, named A, B and C with respectively C_{Er} of 0.05, 0.3, and 1.4 at.% (corresponding to 2.8×10^{19}, 1.7×10^{20} and 7.8×10^{20} cm^{-3}), were elaborated under NH_3 atmosphere on an Si bulk substrate. The Er concentrations and Si contents were determined by Rutherford backscattering (RBS) analysis and the Si concentration of the three samples was approximately 43–44.8 at.%, depending on the introduced amount of Er (C_{Er}). After growth, the samples were annealed in a quartz tube furnace under forming gas (N_2/H_2 95/5) in order to increase the number of photons emitted by the Er ions and to improve the optical properties of the SiO:Er layers. Thermal annealing is generally known to allow the formation of Er–O complexes in order to help the Er^{3+} ions to become optically active. Each sample was annealed at different temperatures (T_a) in the range 500–1050 °C during 1 h in order to study the influence of the post-growth annealing process on the optical properties of the SiO:Er layers.

PL measurements and time-resolved PL were carried out by pumping the samples with the 364 nm line of an Ar^+ laser. We note that, in that case, we preferentially excite the Si-ncs and the LCs into the SRO:Er layers [4, 11], which then transfer energy to the nearby Er ions. The PL signal collected above the excited region under continuous laser excitation is focused on the entrance slits of an infrared spectrometer equipped with a cooled InGaAs photodiode array. Luminescence lifetime measurements were performed by chopping the laser with an acousto-optic modulator at a frequency of 43 Hz with a laser pulse of 5 ms. The decay of luminescence at 1.535 μm was monitored with an infrared InGaAs photomultiplier (PM) tube coupled to a photon counting system. The overall time resolution of the system is less than 100 ns. Effective Er excitation cross section σ_{eff} was determined by measuring the rise and fall time of the 1.535 μm Er^{3+} emission with a numerical oscilloscope connected to the output of the PM as a function of the pumping flux at 364 nm.

The microstructure of the Er-doped SiO layers was investigated by transmission electron microscopy (TEM). High resolution and energy-filtered transmission electron microscopy (HRTEM and EFTEM) images were realized on a JEOL 3010 microscope equipped with a Gatan imaging filter (GIF). EFTEM images were done by selecting the Si plasmon edge near 17 eV. The slit size was 5 eV. Cross sections were observed. EFTEM images allow measuring the size and density of the amorphous Si nanoclusters in the SiO matrix, which act as sensitizers for the Er^{3+} ions. HRTEM images allow determining if the Si nanoclusters are partly crystalline, i.e. if they are nanocrystals or not. By these techniques, we observed the evolution of the microstructure of the SiO films on increasing the annealing temperature T_a.

3. Results and discussion

3.1. Microstructure of the SiO:Er films deposited under NH_3

In figure 1 typical EFTEM images are shown for sample B for three different annealing temperatures under forming gas (a) 500 °C, (b) 850 °C and (c) 1050 °C. White areas of the EFTEM images, realized with the Si plasmon edge at 17 eV,

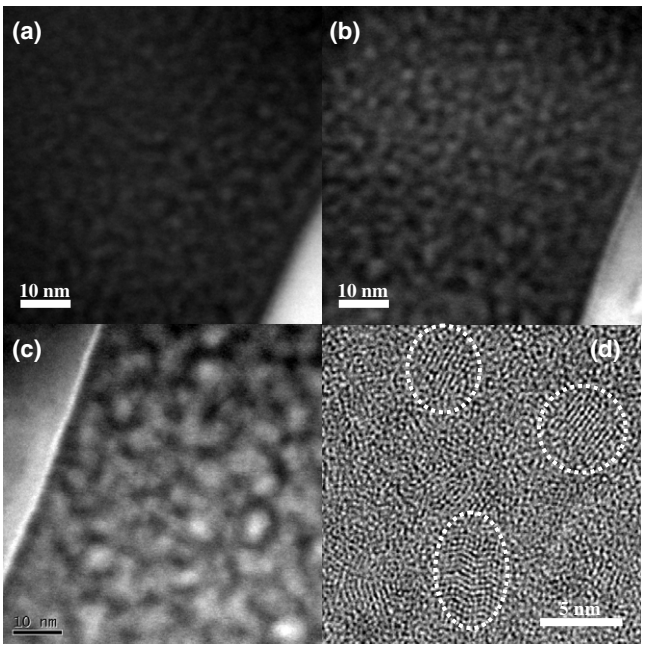

Figure 1. EFTEM images for Er-doped SiO films annealed at (a) 500 °C, (b) 850 °C and (c) 1050 °C. (d) HRTEM image of SiO:Er layer annealed at 1050 °C showing the presence of Si nanocrystals.

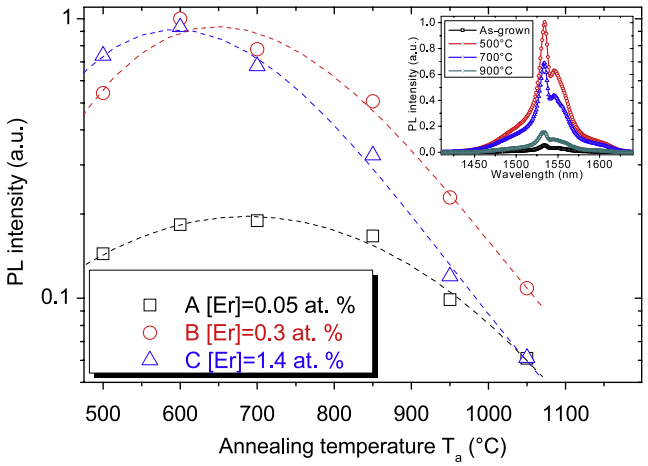

Figure 2. Room-temperature PL intensity at 1535 nm for the samples A, B and C with various Er concentrations (0.05, 0.3 and 1.4 at.%) as a function of annealing temperature T_a. The inset of the figure shows the typical Er^{3+} emission spectra in the SiO matrix as a function of T_a. Dashed lines are only guides for the eyes.

correspond to Si-rich regions, i.e. Si nanoclusters, whether they are crystalline, partly crystalline, what are called nanocrystals, or amorphous. From these images, it is possible to evaluate the approximate size and density of Si nanoclusters. We obtain an Si nanocluster density of approximately 2.7×10^{18} cm^{-3} for $T_a = 500$ and 850 °C, and 10^{18} cm^{-3} for $T_a = 1050$ °C. After annealing at 1050 °C highly crystallized Si nanoclusters are observed, as shown by white circles in figure 1(d), with an increase in cluster size (approximately up to 8 nm compared to 3 nm at 850 °C). It is interesting to note that the density of the Si-ncs in the SiO matrix is constant between 500 and 850 °C (2.7×10^{18} cm^{-3}) then decreases to 10^{18} cm^{-3} for $T_a =$ 1050 °C at which bigger nanoclusters and nanocrystals grow. The main difference between the microstructures of SiO:Er layers annealed at a temperature between 500 and 850 °C is the higher contrast of Si-ncs for $T_a = 850$ °C compared to 500 °C, indicating that these Si-ncs contain more silicon at 850 °C. In order to have more precise information on the composition of the Si-ncs, more investigations are needed but this is not under the scope of this paper. We note that the values measured here are in good agreement with previously reported results [4, 15] where Si-ncs density varies from 1.3×10^{19} to 2×10^{18} cm^{-3} for T_a varying between 400 and 1100 °C.

3.2. Optical properties of the SiO:Er films deposited under NH_3

Figure 2 shows the PL intensity measured at 300 K as a function of the post-growth annealing temperature for the three samples A, B and C with different C_{Er} (0.05, 0.3 and 1.4 at.%). The inset of figure 2 shows the typical PL spectra of Er^{3+} ions in the SiO layer deposited under NH_3 before and after annealing. The excitation photon flux at 364 nm was 2×10^{18} ph cm^{-2} s^{-1}. The PL intensity increases between 500 and 600 °C for samples B and C, then decreases by a factor of 2 (sample B) and 3 (sample C) from 600 to 850 °C. It further decreases by a factor of 5 for T_a higher than 850 °C. On the other hand, the PL intensity of sample A, with the lowest Er concentration, slightly increases from 500 to 700 °C, then decreases by a factor of 2.7 for T_a higher than 850 °C. This result, in good agreement with the previously reported results for such matrices [16, 17], has been attributed either to the decrease of the Si sensitizer density or Er clustering or cooperative up-conversion for high T_a and high C_{Er}. We note that the decrease by a factor of 3 of the density of Si-ncs between 850 and 1050 °C, as observed by EFTEM, could partially explain the evolution of the PL intensity with T_a.

As illustrated by the inset of figure 3 in the case of sample A, the experimental PL decay time curves for all samples exhibit a stretched exponential shape $I(t) = I_0 \exp(-(t/\tau)^\beta)$, which is commonly measured in Er-doped SRO matrices with high Si content [18–20]. By fitting the data (dots) with the stretched exponential function (continuous lines), the measured values of the decay time τ and the dispersion factor β for all samples as a function of T_a are reported in figure 3. For samples A and B with lower C_{Er}, the decay lifetime τ values are higher compared to sample C. This effect of concentration is explained by the Er clustering or the mechanism of cooperative up-conversion which become important non-radiative channels for Er^{3+} as the C_{Er} exceeds (2–4) $\times 10^{20}$ cm^{-3} [21, 22]. Thus, sample C, with an Er concentration of 8×10^{20} cm^{-3}, is in that case. Its decay lifetime τ is constant for T_a higher than 600 °C. The τ values for sample B increase from 0.3 to 0.9 ms for T_a between 600 and 850 °C, then decrease to 0.7 ms for 950 and 1050 °C annealing treatments compared to sample A where the decay lifetime increases from 0.3 to 1.1 ms from 500 to 1050 °C. The lifetime behaviour of samples A and B is explained by taking under consideration the effect of the thermal treatment on the sensitizing properties of the SiO matrix and the optical

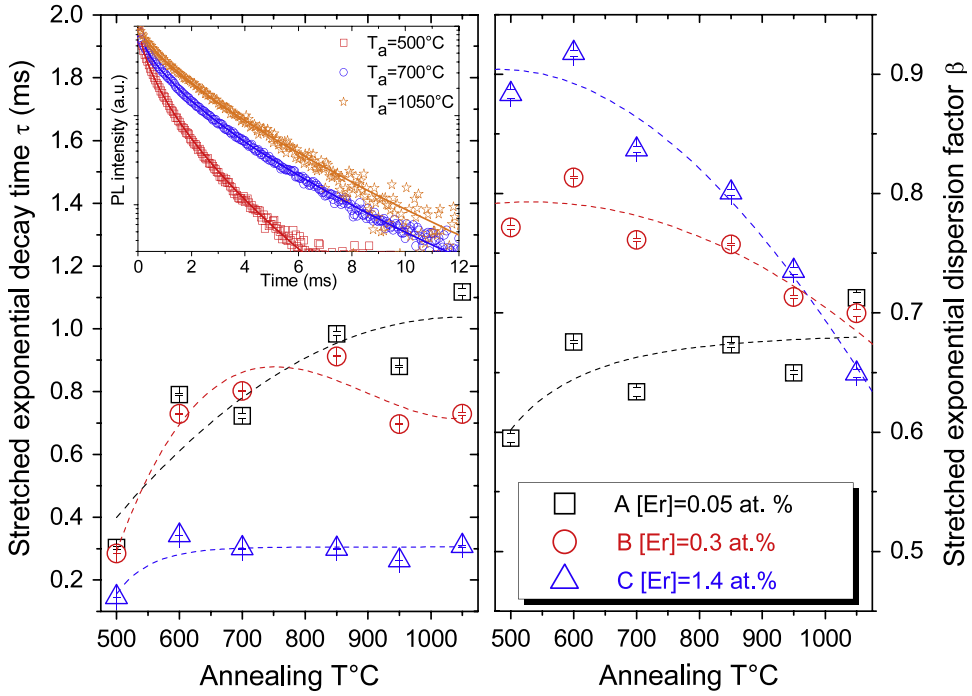

Figure 3. Decay time τ and dispersion factor β obtained by fitting the experimental PL decay curves with a stretched exponential function for samples A, B and C (Er 0.05, 0.3 and 1.4 at.%) as a function of the annealing temperature. (inset) PL decay time at 1535 nm for sample A (Er 0.05 at.%) for three different annealing temperatures T_a: measured (symbols) and simulated (lines) with a stretched exponential function $I(t) = I_0 \exp[-(t/\tau)^{\beta}]$. Dashed lines are only guides for the eyes.

activity of the Er ions. Indeed, the lifetime evolution as a function of the annealing temperature is governed by two competitive mechanisms: on the one hand the reduction of the non-radiative defects (generally removal of defects, relaxation of bond angles and reduction of bond length distortions) and the optical activation of the Er ions, and on the other hand the modification of the nature of the Er sensitizers in the SiO matrix and the clustering of Er ions in non-radiative centres or ESA, depending on the Er concentration. Indeed, as shown in figure 2 the Er^{3+} PL intensity at 1.54 μm for all samples slightly decreases between 700 and 850 °C then strongly decreases from 850 to 1050 °C. This result could be surprising taking into account what could be expected by the lifetime results presented in figure 3. Generally, a longer decay time τ indicates a reduction of the non-radiative transition rate and would result in an increased PL intensity as: $\tau = 1/(W_r + W_{nr})$, where W_r is the radiative rate and W_{nr} is the non-radiative rate due to multiphonon decay and energy transfer from Er^{3+} upper energy levels [23] or other competitive non-radiative mechanisms introduced by the Si excess in the oxide matrix. For example, in figure 3 the decay time τ of sample C increases from 500 to 600 °C, resulting in an increase of the PL intensity but does not vary significantly for T_a higher than 600 °C, which would result in a constant PL intensity. But this is not the case in figure 2. This behaviour could firstly be explained by a decrease of the number of Er^{3+} ions, which could be excited by indirect excitation at 364 nm via the Si nanostructures due to the reduction of the density of sensitizers with the increase of T_a. As shown in figure 1, the nature of the Si-ncs measured by EFTEM changes for T_a between 500 and 850 °C with the appearance of Si-ncs with a higher Si content and their density decreases for T_a higher than 850 °C. As a result, the reduction in density of the sensitizers induces a reduction of the number of Er^{3+} ions which could be excited and also a decrease in the PL intensity. For samples A and B, the decrease in the number of indirectly excited Er^{3+} ions is at the origin of the decrease of the PL intensity but with a different factor of decrease due to the different concentration of Er^{3+} ions introduced in each sample.

The dispersion factor β, which reflects the distribution of time constants in the system related to the indirect bandgap, to the finite size distribution of the Si-ncs and to the strong distance dependence of the nc–Er interaction [20], decreases from 0.92 to 0.65 and 0.81 to 0.7 for, respectively, samples B and C with the highest C_{Er} (0.3 and 1.4 at.%). This effect is well explained by the evolution of the nature of Er^{3+} sensitizers in the SiO matrix as T_a is increased. As reported in [4], when T_a is varied from 600 to 1100 °C, the composition of the SRO matrix is changing from a high density of LCs, for $T_a = 600$ °C, to a progressively reduced density in favour of the formation of Si-ncs, as T_a is increased to 900 °C, and finally Si nanocrystals for higher T_a up to 1100 °C. As previously shown in figure 1, EFTEM and HRTEM images of the SiO samples presented in our study are in good agreement with this result. Moreover, the evolution of the SiO film follows three stages while T_a is increased [15]: a single SiO phase for $T_a < 400$ °C in which amorphous Si-ncs appears and becomes larger for T_a between 400 and 800 °C and starts crystallizing at a critical temperature between 800 and 900 °C resulting in a higher distribution of Si sensitizer sizes in the SiO

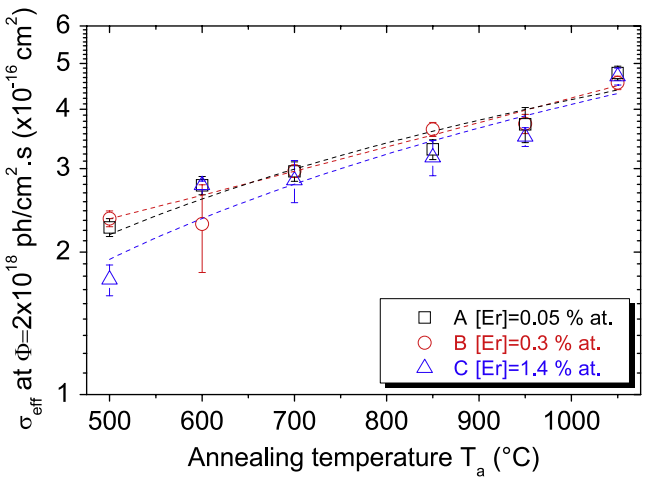

Figure 4. 1.535 μm Er^{3+} effective excitation cross sections σ_{eff} for samples A, B and C as a function of the annealing temperature T_a at a photon flux of 2×10^{18} ph cm^{-2} s^{-1}. Dashed lines are only guides for the eyes.

matrix. This explains the dispersion factor behaviour measured as a function of T_a for samples B and C. As a result, the higher distribution of Si sensitizers when T_a is increased is the first explanation of the behaviour of β for samples B and C. However, for sample A, with the lowest C_{Er}, the dispersion factor β slightly varies from 0.6 to 0.71 for T_a between 500 and 1050 °C. As shown in figure 3 (right) for T_a between 500 and 950 °C, the values of β depend on C_{Er} of the sample. As a result, in this range of T_a, when C_{Er} is decreased, the dispersion factor is lower. For $T_a = 1050$ °C the values of β tend towards a similar value around 0.7. The behaviour of β is also explained by the evolution with T_a of the distribution of the size and nature of the sensitizers and the dependence of β with C_{Er}. The dependence of β with C_{Er} is a result of the higher distribution of the Er-sensitizer distance when the number of emitting Er ions is reduced due to a lower introduced C_{Er} or a decrease of the number of excited Er^{3+} ions when T_a is increased. This is explained in terms of the number of optically active Er^{3+} ions which could be excited through Si sensitizers (N^*_{Er}). As previously reported the sensitization of Er^{3+} by Si-ncs is strongly distance-dependent [7, 17], and only a few Er^{3+} ions can be sensitized by each Si-ncs in the matrix [11, 24]. Thus, in the case of a limited number of optically active Er^{3+} ions in the matrix, for low C_{Er}, Er^{3+} ions which can be sensitized by the Si-ncs are in a more dispersed range of distance from the Si-ncs resulting in lower β values. As a result, the variations of the measured β values, as a function of T_a, are correlated to an increase of the different Er sites, i.e. different local environments or positions of Er atoms (number of O coordination and Er–O interatomic distance), present in these samples which seem to depend on C_{Er} and T_a.

To clarify this last point concerning the number of excited Er^{3+} in the samples, in figure 4 are plotted the effective Er excitation cross sections σ_{eff} at a photon flux of 2×10^{18} ph cm^{-2} s^{-1} at 364 nm for each sample as a function of T_a. The values of σ_{eff} are extracted from the measurements of the rise (τ_r) and decay times (τ_d) of the Er^{3+} PL at 1.535 μm as a function of the photon flux Φ following the well-known relation $1/\tau_r - 1/\tau_d = \sigma_{eff}\Phi$ [25]. σ_{eff} are orders of magnitude higher than the Er^{3+} cross section in a pure silica matrix ($\sim 10^{-21}$ cm^2), indicating that the excitation of Er^{3+} ions at 364 nm effectively occurs indirectly through the sensitizers in the SiO matrix. For all the samples, at this photon flux, σ_{eff} is similar and follows the same behaviour as T_a is increased. The increase of σ_{eff} is due to the increase of the absorption cross section of the sensitizers for the Er^{3+} ions due to the evolution of the SiO matrix when T_a is increased, and the appearance of an increasing number of pure Si domains [17]. It is now interesting to deduce from these values the relative number of excited Er^{3+} ions N^*_{Er} for samples A, B and C as a function of T_a. N^*_{Er} is proportional to the ratio of the PL intensity I_{PL} and $\sigma_{eff} \times \tau_d$ [4, 18] following the relation: $I_{PL} \propto \sigma_{eff} \times \Phi \times \tau_d \times N^*_{Er}$. In figure 5, we plot N^*_{Er} as a function of T_a. N^*_{Er} noticeably decreases when T_a is increased. This decrease is of a factor of 84, 30 and 15, depending on C_{Er} decreasing from 1.4 to 0.05 at.%. This result indicates that a major part of the Er^{3+} in the layers, with highest T_a, cannot be sensitized. This could be a result of Er clustering (optically inactive Er aggregates with Er–Er coordination) or pair-induced quenching mechanism (PIQ or inhomogeneous up-conversion) [26], depending on the introduced C_{Er} due to Er–Er interaction. The PIQ mechanism is due to two excited Er ions which can interact, yielding one Er ion in the $^4I_{9/2}$ state, which rapidly decays to the first excited state, and one Er ion in the ground state. This cooperative up-conversion effect usually results in a shortening of the Er decay rate and is usually called pair-induced quenching (PIQ). If we compare N^*_{Er} regarding the initial C_{Er} of sample C, we can compare the relative emitting fraction N^*_{Er}/N_{Er} between the three samples (figure 5 right). For samples A and B with the lowest C_{Er}, we can expect a higher inverted fraction than in sample C. These findings are partially explained by previously reported results where the highest Er^{3+} PL was observed for T_a lower than 800 °C where a high density of Si sensitizers can excite a higher number of Er ions compared to a sample annealed at higher T_a where the density of Si sensitizers decreases [8]. Moreover, EFTEM investigations showed the decrease of the Si-ncs density for the highest temperature of 1050 °C, but the main difference between 500 and 850 °C is the evolution of the nature of the sensitizers where more pure amorphous Si domains appear when T_a is increased, and thus at the same time the environment around the Er^{3+} ions is changing. We note that the sharp decrease of N^*_{Er} suggests that, when T_a is increased, either Er^{3+} ions become optically inactive due to Er precipitation or that the Er^{3+} excitation process is affected by the evolution of the nature of the sensitizers in the SiO matrix. This last hypothesis is supported by the Izzedin *et al* model of energy transfer in Er-doped SiO_2 sensitized with Si nanocrystals. In this model, the apparent loss of optical activity in the majority of Er dopants upon sensitization with Si nanocrystals is attributed to the appearance of a very efficient energy exchange mechanism between Si nanocrystals and Er^{3+} ions [27]. The Er^{3+} ions are very efficiently excited by an energy exchange via an intraband Auger transfer process between the Si nanocrystals and Er^{3+} ions but also undergo

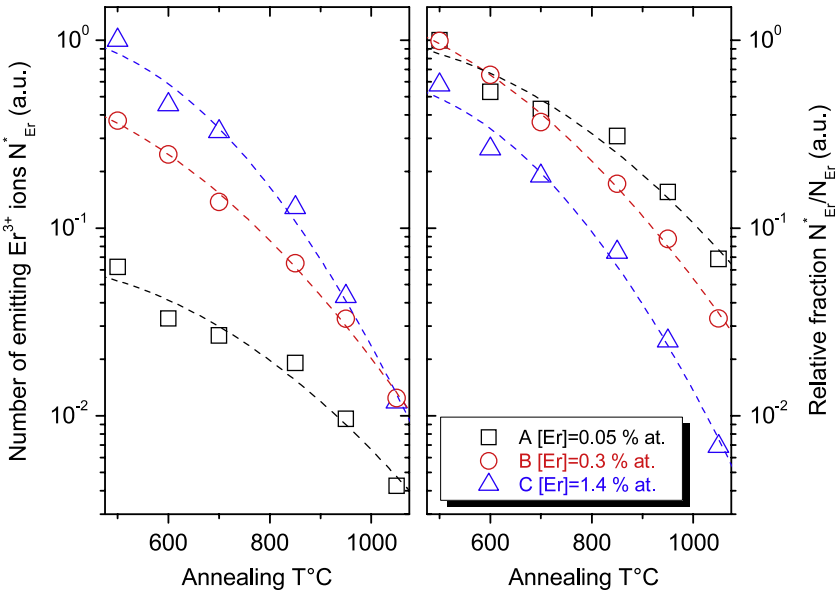

Figure 5. (left) Number of excited Er^{3+} ions N^*_{Er} via indirect excitation as a function of the annealing temperature T_a for samples A, B and C and (right) comparison of the relative fraction of emitting Er^{3+} ions in the SRO layers N^*_{Er}/N_{Er} between samples A, B and C as a function of T_a. Dashed lines are only guides for the eyes.

a very effective excitation back-transfer process preventing the excited Er^{3+} ions to contribute to PL. In our study the behaviour of N^*_{Er} is in accordance with these recent findings for which the appearance of more pure Si domains (or Si-ncs) when T_a is increased and then nanocrystals at high temperature will make this transfer process more and more important. But at this point it is not possible to conclude on the exact origin of the behaviour of N^*_{Er} at high annealing temperatures. Indeed, the local environment of Er^{3+} ions is known to play a crucial role in their emission efficiency and could evolve when T_a is increased.

3.3. EXAFS analysis of the local order around Er^{3+} ions in the SiO:Er films deposited under NH_3

In the previous sections we have shown that the PL intensity of Er^{3+} ions at 1.5 μm in the SiO matrix decreases as T_a is increased from 600 to 1050 °C. The excitation of Er^{3+} ions at 364 nm effectively preferentially occurs indirectly via the excess-silicon-related sensitizers (Si-ncs and LCs) as shown by the measurement of the Er effective excitation cross sections σ_{eff}. Indeed, σ_{eff} are orders of magnitude higher than the Er^{3+} direct excitation resonantly with its 4f energy levels. The origin of this decrease of PL is attributed to the reduction of the number of excited Er^{3+} ions when T_a is increased independently of the initial C_{Er}. We could identify several origins for this effect:

(i) the decrease of the density of sensitizers for Er^{3+} ions when T_a is increased, as shown by EFTEM investigations, and the limited number of Er^{3+} ions excitable per sensitizer,
(ii) the appearance of more pure Si-ncs between 500 °C and 850 °C, followed by Si nanocrystals for T_a as high as 1050 °C which would induce a back-transfer process, preventing a major part of the Er^{3+} ions from emitting photons,
(iii) Er clustering or pair-induced quenching mechanism (PIQ or inhomogeneous up-conversion) depending on the introduced C_{Er} due to Er–Er interaction when T_a is increased,
(iv) the modification of the local chemical environment around Er^{3+} ions which could have a large influence on the $^4I_{13/2} \rightarrow {}^4I_{15/2}$ transition of erbium responsible for the 1.54 μm light emission.

In order to investigate deeply the origin of the evolution of N^*_{Er} as a function of T_a, an EXAFS experiment was performed at the Italian beamline GILDA of the European Synchrotron Radiation Facility [28]. For this experiment an SiO:Er sample with a C_{Er} of 0.4 at.% similar to the previous samples was measured as a function of T_a between 400 and 1050 °C. We note that the composition of this sample is that which presents the best PL intensity at 1.54 μm. The details of the experimental procedure and the EXAFS quantitative analysis by the GNXAS code are described elsewhere [7]. In figure 6, from the EXAFS analysis, we can plot as a function of T_a the quantitative results on the local environment around the erbium ions:

(i) the number N_O of oxygens in the first shell of Er and their distance R_{Er-O} from Er,
(ii) the Er to Si distance R_{Er-Si}.

The model considers one single Si atom for each O neighbour. First of all, the first coordination shell in all samples follows the behaviour observed in oxygen-poor matrices [7], i.e. the R_{Er-O} distance shrinks for smaller Er–O coordination number N_O (figure 6(c)). As shown in figure 6(a), the second shell distance R_{Er-Si} does not seem to vary significantly with

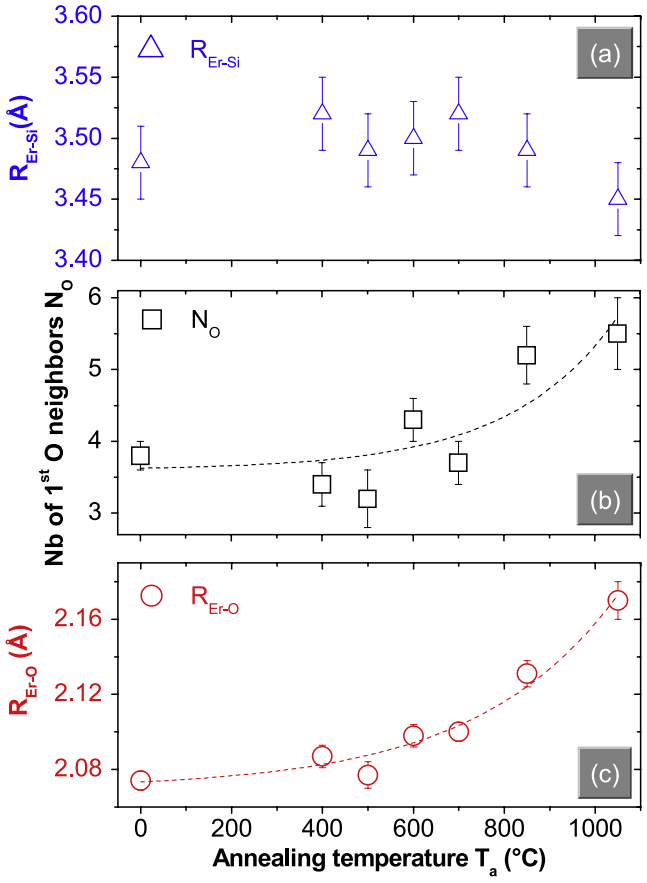

Figure 6. (a) Er–Si interatomic distance as a function of the annealing temperature T_a deduced from EXAFS analysis. (b) Number of O N_{Er-O} in the first shell of Er atoms as a function of the annealing temperature T_a. The local order around Er atoms evolves from a low coordination of ∼3.4 O to a higher coordination of ∼5.5 O as T_a is increased from 400 to 1050 °C. (c) Er–O interatomic distance R_{Er-O} as a function of the annealing temperature T_a. The local order around Er atoms evolves from a low coordination of ∼3.4 O at 2.07 Å to a higher coordination of ∼5.5 O at 2.17 Å as T_a is increased from 400 to 1050 °C. Dashed lines are only guides for the eyes.

T_a. Moreover, from this analysis, we can conclude that there is no Er clustering in the samples with no signature of Er–Er bonds and no Er_2O_3 configuration which was one possible explanation of the decrease of N^*_{Er} with T_a. But, as shown in figures 6(b) and (c), there is a strong correlation between N_O, the first shell bond length R_{Er-O} and the increase of T_a. Indeed, as shown in figure 5, N^*_{Er} decreases as T_a increases whereas at the same time the average Er^{3+} configuration in the matrix evolves. As previously shown, the behaviour of N^*_{Er} as a function of T_a is not due to Er clustering or the Er_2O_3 compound in the layers. But the decrease of N^*_{Er} is related to the evolution of the local configuration of the Er ions. As T_a is increased, the mean configuration of Er atoms moves from 3.2–3.4 O at 2.08–2.09 Å to 5.5 O at 2.17 Å. The threefold Er coordination has a lower symmetry than the sixfold coordination increasing the probability of the normally forbidden $^4I_{13/2} \rightarrow {}^4I_{15/2}$ transition. Indeed, the $^4I_{13/2} \rightarrow {}^4I_{15/2}$ transition in the free atom is forbidden, and only when the crystal field of the host breaks inversion symmetry and mixes states of opposite parity is the transition allowed. The transition probability is determined by the magnitude of the crystal field which depends on the symmetry of the ligands around Er. In that case, it is not surprising that more shorter Er–O ionic bonds, as in the case of low T_a where we find R_{Er-O} = 2.08–2.09 Å, are at the origin of a more intense Er^{3+} PL and a higher number N^*_{Er} of emitting Er^{3+} ions [29]. We note that, in the case of the Er_2O_3 compound, we find 6 O at 2.26 Å with an octahedral cage around Er atoms [30, 31]. By this result, we can conclude that, in addition to cooperative up-conversion or ESA and the reduction of the density of Si sensitizers in the SRO matrix as T_a is increased, an explanation of the limited number of Er^{3+} emitters N^*_{Er} is due to the evolution of the local Er^{3+} bonding configuration. This configuration moves from a lower to a higher O symmetry environment resulting in a lower transition probability. At the same time a lower transition probability results in a longer radiative lifetime and is favourable for a higher probability of non-radiative back-transfer process to Si-ncs. This result is also very important for future improvement of the engineering of the material and in order to improve the inverted fraction of Er^{3+} in the SRO matrix. For optical gain and light amplification applications it would now be interesting to study the absorption of the Er^{3+} ions which cannot emit light. Indeed the main limitation of the EXAFS investigations is that it gives mean information on all the Er population and not only the optically active Er^{3+} ions. In order to be able to conclude on the effect reported here it would now be interesting to analyse only the emitting population which is involved in light emission in our material. We note that a recent report [24] showed that a part of the population of Er^{3+} does not participate in the 1.54 μm emission or absorption in the SRO matrix. This is probably due to the local configuration around these ions for which the Er 1.54 μm transition should be partially forbidden.

4. Conclusion

In summary, we have studied the optical properties of Er^{3+} ions incorporated with Si sensitizers in an SRO matrix as a function of the Er concentration and the annealing temperature of the films. The 1.54 μm Er^{3+} photoluminescence intensity and lifetime under indirect excitation are shown to be highly dependent on the elaboration parameters. The number of emitting Er ions through indirect excitation via the sensitizers in the SRO matrix decreases as the annealing temperature is increased from 500 to 1050 °C. In particular, EXAFS investigations indicate that, from 500 to 1050 °C, the local order around Er atoms changes from a low to a high O coordination in the first shell. This evolution becomes detrimental to the probability of the 1.54 Er^{3+} transition. As a result, whereas the annealing treatment contributes to the reduction of the non-radiative defects in the SRO matrix, which improves the photoluminescence lifetime, it reduces the number of Er^{3+} which can emit light. Thus, depending on the required application, the elaboration parameters of such a material will have to be adapted in order to obtain either the highest PL intensity due to the Er^{3+} ions or the highest fraction of Er^{3+} ions invertible in the matrix.

References

[1] Coffa S, Polman A and Schwartz R N 1996 *Mater. Res. Soc. Symp. Proc. Rare Earth Doped Semiconductors II (San Francisco, April 1996)* vol 422, ed S Coffa, A Polman and R N Schwartz (Pittsburgh, PA: Materials Research Society) pp 369

[2] D'Acapito F, Mobilio S, Scalese S, Terrasi A, Franzò G and Priolo F 2004 *Phys. Rev.* B **69** 153310

[3] Kenyon A J, Trwoga P F, Federighi M and Pitt C W 1994 *J. Phys.: Condens. Matter* **6** L319

[4] Savchyn O, Ruhge F R, Kik P G, Todi R M, Coffey K R, Nukala H and Heinrich H 2007 *Phys. Rev.* B **76** 195419

[5] Pacifici D, Franzò G, Priolo F, Iacona F and Dal Negro L 2003 *Phys. Rev.* B **67** 245301

[6] Fujii M, Yoshida M, Kanzawa Y, Hayashi S and Yamamoto K 1997 *Appl. Phys. Lett.* **71** 1198

[7] Noé P, Salem B, Delamadeleine E, Jalabert D, Calvo V, Maurizio C and D'Acapito F 2007 *J. Appl. Phys.* **102** 103516

[8] Franzo G, Boninelli S, Pacifici D, Priolo F, Iacona F and Bongiorno C 2003 *Appl. Phys. Lett.* **82** 3871

[9] Franzo G, Pecora E, Priolo F and Iacona F 2007 *Appl. Phys. Lett.* **90** 183102

[10] Pellegrino P, Garrido B, Arbiol J, Garcia C, Lebour Y and Morante J R 2006 *Appl. Phys. Lett.* **88** 121915

[11] Oton C J, Loh W H and Kenyon A J 2006 *Appl. Phys. Lett.* **89** 031116

[12] Lee H, Shin J H and Park N 2005 *Opt. Express* **13** 9881

[13] Han H-S, Seo S-Y and Shin J H 2001 *Appl. Phys. Lett.* **79** 4568

[14] Salem B, Noé P, Mazen F, Calvo V and Hadji E 2006 *J. Lumin.* **121** 242–4

[15] Wang J, Wang X F, Li Q, Hryciw A and Meldrum A 2007 *Phil. Mag.* **87** 11–27

[16] Fukata N, Morihiro H, Shirakawa R, Murakami K, Mitome M and Bando Y 2007 *J. Appl. Phys.* **102** 114309

[17] Wora Adeola G, Rinnert H, Miska P and Vergnat M 2007 *J. Appl. Phys.* **102** 053515

[18] Franzo G, Pecora E, Priolo F and Iacona F 2007 *Appl. Phys. Lett.* **90** 183102

[19] Pavesi L and Ceschini M 1993 *Phys. Rev.* B **48** 17625

[20] Kenyon A J, Wojdak M, Ahmad I, Loh W H and Oton C J 2008 *Phys. Rev.* B **77** 035318

[21] Gourbilleau F, Dufour C, Levalois M, Vicens J, Rizk R, Sada C, Enrichi F and Battaglin G 2003 *J. Appl. Phys.* **94** 3869

[22] Gourbilleau F, Levalois M, Dufour C, Vicens J and Rizk R 2004 *J. Appl. Phys.* **95** 3717

[23] Pan Z, Morgan S H, Dyer K, Ueda A and Liu H 1996 *J. Appl. Phys.* **79** 8906

[24] Lee P A, Citrin P H, Eisenberger P and Kincaid B M 1981 *Rev. Mod. Phys.* **53** 769

[25] Navarro-Urrios D, Daldosso N, García C, Pellegrino P, Garrido B, Gourbilleau F, Rizk R and Pavesi L 2007 *Japan. J. Appl. Phys.* **46** 6626–33

[26] Quimby R S, Miniscalco W J and Thompson B 1994 *J. Appl. Phys.* **76** 4472

[27] Izzedin I, Timmerman D, Gregorkiewicz T, Moskalenko A S, Prokofiev A A, Yassievich I N and Fujii M 2008 *Phys. Rev.* B **78** 035327

[28] d'Acapito F *et al* 1998 *ESRF Newsletter* **30** 42

[29] Adler D L, Jacobson D C, Eaglesham D J, Marcus M A, Benton J L, Poate J M and Citrin P H 1992 *Appl. Phys. Lett.* **61** 2181

[30] Terrasi A, Franzò G, Coffa S, Priolo F, D'Acapito F and Mobilio S 1997 *Appl. Phys. Lett.* **70** 1712

[31] Bian L-F, Zhang C G, Chen W D, Hsu C C and Shi T F 2006 *Appl. Phys. Lett.* **89** 231927